

Effect of plasma-assisted N₂O/Ar oxidation on TOPCon solar cells

Jiabin Huang, Zengchao Zhao^{*}, Ming Li, Jun Chen, Xiaorong Zhou, Xinxin Deng, Bin Li, Kailin Shen, Qiuyun Cheng, Xianwu Cai

Hunan Red Solar Photoelectricity Science and Technology Co., Ltd., National Engineering Research Center of Photovoltaic Equipment(NCPVE), Changsha, 410000, China



ARTICLE INFO

Keywords:

SiO_x
TOPCon
Passivated contact
Plasma-assisted

ABSTRACT

N₂O/Ar gas mixture are used to deposit ultra-thin silicon oxide (SiO_x) layer by plasma enhanced chemical vapor deposition (PECVD), which is used as the tunneling oxide layer in the TOPCon (tunnel oxide passivated contacts) structure. It is found that the N₂O/Ar flow ratios strongly affect the properties of SiO_x layer, such as deposition rate, the resistance of high temperature, passivation quality, etc., thus significantly affect the properties of polysilicon passivated contact structures and the efficiency of TOPCon solar cells. The deposition rate of SiO_x layer and contact resistivity of SiO_x/poly-Si(n⁺)/SiNx:H structure decrease with the increases of Ar flow. However, there is an optimal N₂O/Ar flow ratio to obtain the best passivation quality and the champion efficiency. The optimal flow ratio of N₂O/Ar= 5:2 is found, and obtain the optimum thickness of SiO_x and uniform polysilicon passivated contact. The highest minority carrier lifetime (τ) of 5751 μ s, highest implied open circuit voltage (iV_{oc}) of 741.3 mV, lowest single side recombination saturation current density(J_0) of 4.79 fA/cm², contact resistivity($\rho_{contact}$) of 2.23 m Ω /cm² and champion efficiency of 25.06% are obtained at the flow ratio of N₂O/Ar= 5:2.

1. Introduction

In recent years, tunnel oxide passivated contact structure solar cells (i.e. TOPCon) based on doped polysilicon (n⁺-poly-Si) layer and ultra-thin tunneling SiO_x layer are proved to be a promising technology for the next generation of highly efficient industrial silicon solar cells. It will replace the mainstream passivated emitter and back cell (PERC) and double-sided PERC + solar cell, thus attracting more and more attention [1–3]. The photoelectric conversion efficiency of lab-type POLO2 IBC and TOPCon cells are up to 26.1% or more [4,5]. A high quality tunneling SiO_x layer is essential to provide effective chemical passivation and allow selective carrier transport through quantum tunneling and/or pinholes [6–13]. At present, the ultra-thin tunneling SiO_x layer can be prepared by such methods as wet chemical oxidation [6,14,15], high-temperature thermal oxidation [16–18], ozone oxidation [19,20], atomic layer deposition(ALD) [21,22], etc. However, the above methods are limited in their application in industry due to their shortcomings [16,23–25]. The ultra-thin tunneling SiO_x layer prepared by low-pressure chemical vapor deposition (LPCVD) has high density, high temperature stability, and can realize the same tube preparation of oxide layer and amorphous silicon layer. However, the lifetime of quartz tube

is short due to the existence of thermal stress between amorphous silicon and quartz tube, which greatly increases the manufacturing cost of the solar cells. Wet chemical oxidation, ozone oxidation and ALD require an additional step to separate preparation of the oxide layer from the doped amorphous silicon layer, which potentially increase the risk of contamination, in addition to requiring additional equipment [25]. Therefore, researchers are focusing on the plasma-assisted oxidation manufacturing method that combines the growth of ultra-thin tunneling SiO_x layer with the deposition of amorphous silicon layer at present [25–28]. The combination of ultra-thin tunneling SiO_x prepared by plasma-assisted N₂O oxidation and n⁺-poly-Si layer obtained excellent iV_{oc} values as high as 730 mV and corresponding J₀ values as low as 4.3 fA/cm² [25]. Plasma-assisted N₂O oxidation is the decomposition of N₂O into free radicals such as NO*, O*, N* in a vacuum chamber by capacitively coupled plasma (CCP) PECVD method, then the O* react with silicon on the surface to form SiO_x under the electric field [29]. The remote plasma-enhanced chemical vapor deposition (RPECVD) process developed by Lucovsky and colleagues employs He/N₂O remote radio frequency (rf) plasma to grow SiO_x. It has been reported that SiO_x films deposited with He/N₂O have fewer Si-OH defects than those deposited with He/O₂ [30]. In addition, remote plasma-assisted oxidation (RPAO)

* Corresponding author.

E-mail addresses: huangjb@cs48.com (J. Huang), zhaozc@cs48.com (Z. Zhao).

using He/N₂O plasma has the additional benefit of binding N at the Si-SiO_x interface, resulting in improved interface quality [29,31–34]. The introduction of N or other impurities in the interface layer can further improve the electrical properties and thermal stability of poly-Si passivated contact [2]. The importance of He dilution in producing high quality SiO_x films by PECVD has been emphasized by several groups [35, 36]. Smith and Alimonda consider that a large excess of atomic O are critical for obtaining high-quality PECVD oxides and that particle formation can be effectively suppressed by using lower pressures or diluting the reactant inert gas (He or Ar) [37]. Substitution of He by Ar can increase the concentration of atomic O, in addition, mild Ar⁺ bombardment during deposition may lead to greater Si–O–Si bond angle relaxation in the as-deposited film [38]. Therefore, the quality and chemical composition of this ultra-thin tunneling SiO_x layer can be controlled and optimized by introducing Ar and other inert gases into the process of plasma-assisted N₂O oxidation, thus helping us to improve their electrical properties.

In this paper, we present an ultra-thin tunneling SiO_x layer deposition method, which introduced Ar into N₂O and use plasma-assisted N₂O/Ar oxidation (PANAO) method to prepare ultra-thin tunneling SiO_x layer. In addition, we combine the deposition of ultra-thin tunneling SiO_x films and doped amorphous silicon (n⁺-a-Si) films in a single PECVD chamber. This provide a simple, fast and clean method to fabricate polysilicon passivated contacts. Meanwhile, The control of deposition time, process gas flow ratio, deposition pressure, deposition temperature and deposition RF power allow us to control the chemical composition and deposition rate of the ultra-thin tunneling SiO_x layer. PECVD has a faster growth rate (i.e. >1 nm SiO_x was formed in 2 min by plasma-assisted N₂O/Ar oxidation in this paper) than thermal oxidation methods (i.e. a 1.8 nm SiO_x was formed in ~20 min at 650 °C by thermal oxidation of LPCVD [18]). In this work, the types of atoms and molecules excited by electrons during N₂O/Ar plasma discharge are detected by in-situ optical emission spectroscopy (OES), and the relationship between the emission intensities of O atoms and different N₂O/Ar gas flow ratios are investigated. The characteristics of ultra-thin tunneling SiO_x film are studied by full spectral ellipsometry, such as the relationship between the growth rate, uniformity of the SiO_x film with the flow ratio of N₂O/Ar precursor. Subsequently, the relationship between doping concentration of SiO_x/n⁺-poly-Si passivated contact structure and the

flow ratio of N₂O/Ar precursor are researched by electrochemical capacitance voltage (ECV) tester. We also have studied the relationship between the electrical performance and the flow ratio of N₂O/Ar precursor to obtain an optimal SiO_x layer to achieve highly performing passivated contacts. The results indicate that variations in the gas flow ratios can significantly change the atomic O concentration of the ultra-thin tunneling SiO_x layer, which affect the stability and electrical performance of the corresponding poly-Si passivated contacts. Finally, we have studied the effect of N₂O/Ar flow ratio on conversion efficiency of TOPCon solar cells, and obtain the best efficiency.

2. Experimental methods

N-type 158.75*158.75 mm² commercial Czochralski (Cz) silicon wafer (1–2 Ωcm) with thickness of 170±10 μm were used as passivation quality and contact resistivity test samples. N-type 182*182 mm² commercial Czochralski (Cz) silicon wafer (1–2 Ωcm) with thickness of 150 ±10 μm were used for the preparation of solar cell samples. The flow chart of experimental details was shown in Fig. 1. After a saw damage removal step, all samples were textured and then immersed in 10% KOH solution for alkaline polishing and cleaned by standard RCA solutions. The resulting polished wafer were used for SiO_x thickness test and passivation quality test. SiO_x/a-Si (n⁺) stacks were deposited at 480 °C through a tube PECVD system (Hunan Red Solar Photoelectricity Science and Technology Co., Ltd. N₂O(99.9999%) and Ar(99.9999%) were used as precursor gases for SiO_x deposition. SiH₄(99.9999%), Ar and PH₃ (5% diluted in Ar, 99.9999%) were used as precursor gases for a-Si (n⁺) deposition). We had adjusted the N₂O/Ar gas flow ratio over a wide range to ensure that the properties of the SiO_x interfacial layer meets the requirements of the passivated contact structure uniformity and thickness. After the approximate range of the optimal N₂O/Ar gas flow ratio were identified, 7 different SiO_x layers were formed by modifying the gas flow ratio of N₂O and Ar (in slm) with values of 5:0, 5:0.5, 5:1, 5:2, 5:5, 5:8 and 5:10, respectively. The deposition time, deposition pressure and deposition RF power were fixed at 120 s, 150 Pa and 9000 W respectively. Subsequently, about 120 nm a-Si(n⁺) was deposited in the same chamber (deposition conditions: SiH₄/Ar/PH₃=1:5:1, time=900 s, pressure=150 Pa, temperature=480 °C, RF power=10000 W). The thickness of SiO_x films deposited under different N₂O/Ar gas flow ratios

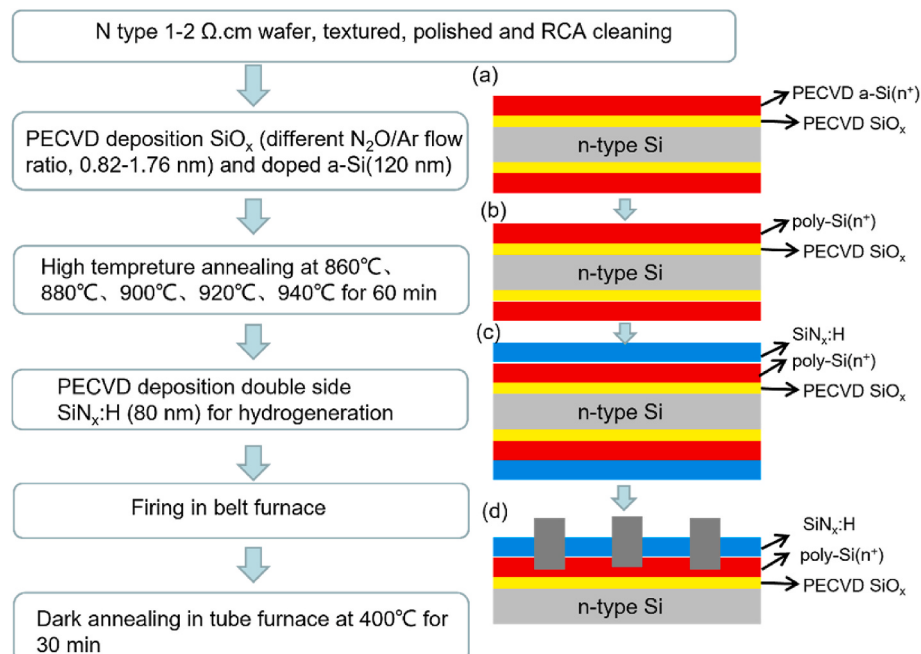


Fig. 1. Flowchart of experimental details and schematic diagram of passivated contact structure.

and thickness of a-Si(n⁺) were measured by full spectral ellipsometry (Elitop ES01), as shown in Fig. 1(a). As the N₂O/Ar gas flow ratios were adjusted, the types of atoms and molecules excited by electrons in the N₂O/Ar plasma were measured by an in-situ optical emission spectroscopy (OES, Horiba, iHR320).

Both passivation quality and contact resistivity test samples prepared under the conditions of different N₂O/Ar gas flow ratios were subject to high temperature annealing processes at 920 °C for 60 min. After the optimal gas flow ratio was obtained, the influence of different annealing temperatures (860 °C/880 °C/900 °C/920 °C/940 °C) on the passivation quality were explored. Four-probe tester (Four Dimensions, Inc, 280SI) was used for studying the function between the sheet resistance (R_{sh}) and N₂O/Ar gas flow ratios and annealing temperatures on the SiO_x/poly-Si(n⁺) structure, as shown in Fig. 1 (b). For the measurement of minority lifetime (τ), implied open circuit voltage (iV_{oc}) and single side saturated recombination current density (J_0), The SiO_x/poly-Si(n⁺)/SiN_x:H passivated contact layers were deposited sympathetically on both sides of silicon wafer, as shown in Fig. 1 (c). The values of τ , iV_{oc} and J_0 were obtained by Quasi-steady-state photoconductance (QSSPC, Sinton WCT-120) at 1-Sun equivalent light intensity, and the excess carrier injection level was $1 \times 10^{15} \text{ cm}^{-3}$. Contact resistivity (ρ_{contact}) was extracted by the method of transmission line method (TLM, Pvtools, TLM-SCAN). The single-sided SiO_x/poly-Si(n⁺)/SiN_x:H structure was designed with 5 busbars and 236 fingers, as shown in Fig. 1 (d). The ρ_{contact} between metal and poly-Si(n⁺) was calculated using the I-V data measured at different gap widths between two electrodes, by which the contribution from the poly-Si layer was removed, and the accurate contact resistivity could be obtained. An electrochemical capacitance-voltage (ECV, WEP Wafer Profile CVP21) was used to measure the dopant concentration profiles of the annealed c-Si/SiO_x/poly-Si(n⁺) structure samples.

3. Results and discussion

3.1. Kinetics of plasma-assisted N₂O/Ar oxidation(PANAO) SiO_x

The average oxidation thickness of SiO_x is gradually decreased from 1.76 nm (N₂O/Ar=5:0) to 0.82 nm (N₂O/Ar=5:10) with the decrease of N₂O/Ar flow ratio under the condition of constant N₂O flow, as evidenced in Fig. 2(a). This may be caused by the addition of Ar diluting the process gases and decreasing the concentration of N₂O, resulting in a reduction of SiO_x thickness. In addition, it can also be seen from Fig. 2(a) that the deposition uniformity of SiO_x is gradually improved (the thickness range of SiO_x decreases from 0.55 nm to 0.17 nm) after adding the Ar into N₂O. The effects of total pressure and deposition temperature on the deposition thickness of SiO_x are shown in Fig. 2(b). The deposition thickness increases with the increase of pressure from 100 Pa to 350 Pa at all temperatures, but the deposition rate become slower at higher pressure, which may be due to the increase of collision frequency between Ar⁺ and N₂O, thus reducing Ar⁺ energy and the yield of O atoms. From Fig. 2 (c), We find that the thickness of SiO_x formed by PANAO growths extremely fast at the first tens of seconds, but then gradually decreases with the extension of time until it reaches the self-saturated thickness, which is consistent with the description in literature [25]. In addition, with the increases of RF power, the growth rate is also accelerated, and the self-saturation thickness increases with the increase of RF power. This can be attributed to increasing RF power provides high energy ionized oxygen atoms to penetrate deeper in the SiO_x, both of which contributes to increasing SiO_x saturation thickness [25].

Fig. 3 shows the spectra of the in-situ OES under the condition of 480 °C, 150 Pa and 9000 W RF power with different N₂O/Ar flow ratios. Many narrow Ar^{*} emission lines are observed in the near infrared between 700 and 900 nm, corresponding to the 3p⁵4p → 3p⁵4s transition [39], as denoted by the asterisks in Fig. 3(a). The intensity of Ar^{*} emission lines increase with the increase of Ar flow. Sharp atomic O emission lines at 777 and 844 nm corresponding to 3p⁵P → 3s²S and

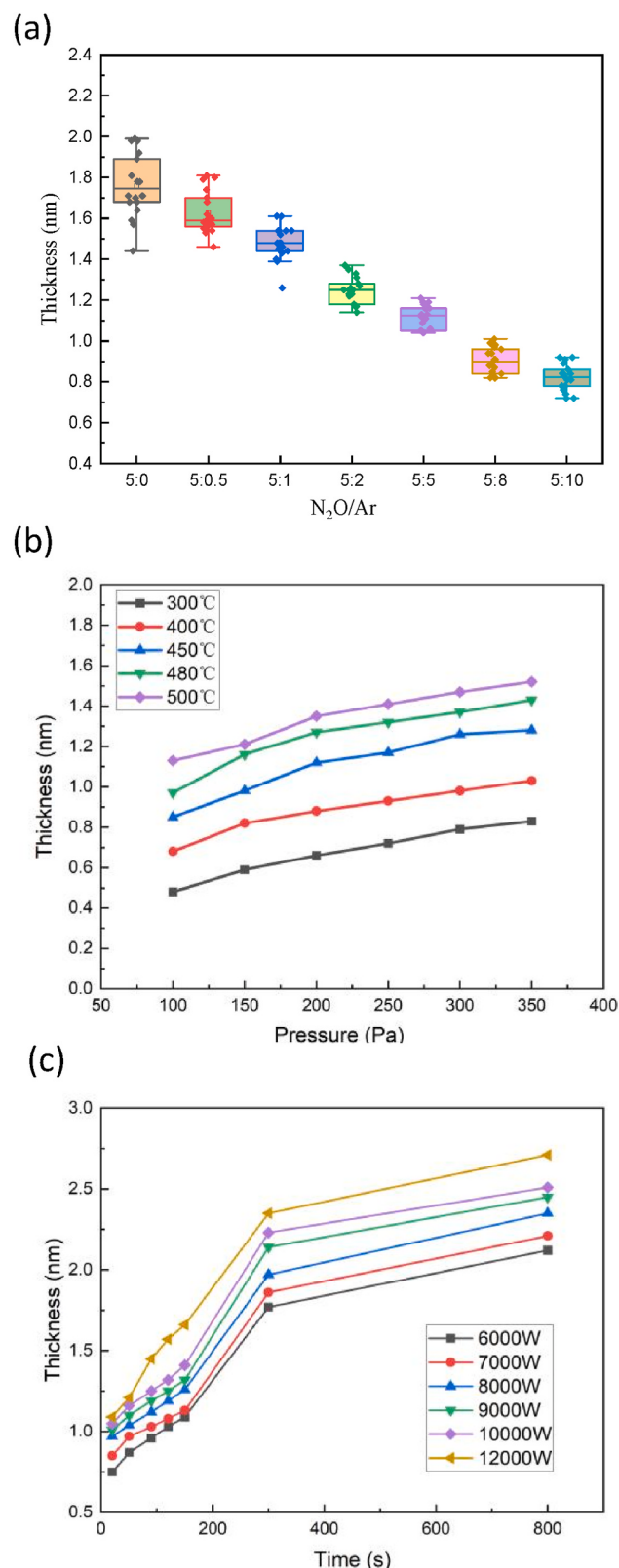


Fig. 2. (a) The relationship between the deposition thickness of SiO_x and the N₂O/Ar flow ratios(time=120 s, pressure=150 Pa, RF=9000 W, T=480 °C); (b) Effects of pressure and substrate temperature on the thickness of PANAO SiO_x layer(time=120 s , RF power=9000 W , N₂O/Ar=5:2); (c) Effects of processing time and RF power on the thickness of PANAO SiO_x layer(T=480 °C, pressure=150 Pa , N₂O/Ar=5:2).

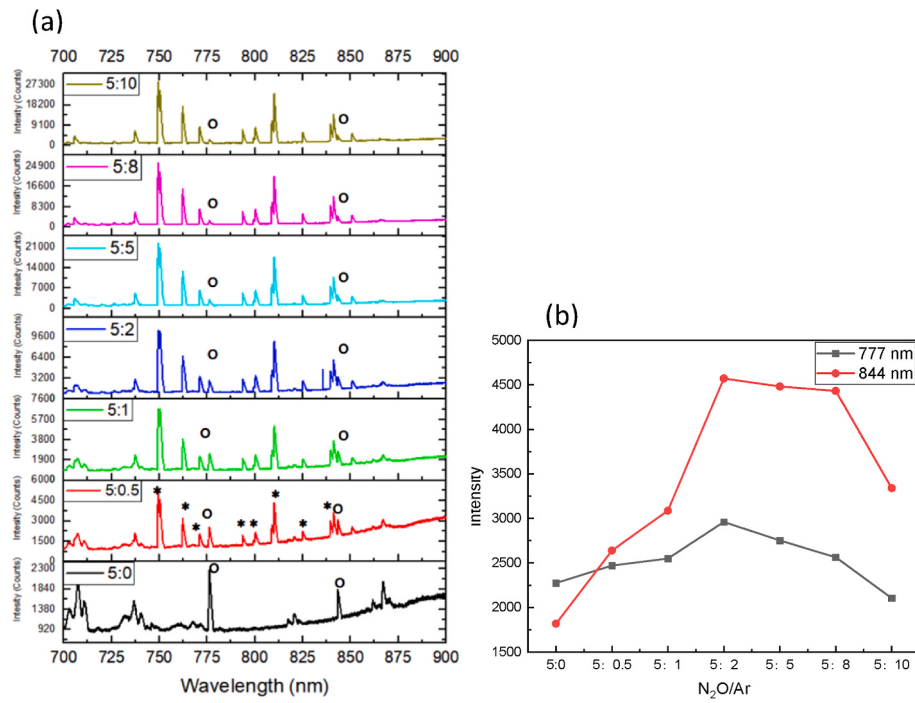


Fig. 3. (a) In-situ OES spectra of different N_2O/Ar flow ratio at $480\text{ }^\circ\text{C}$, 150 Pa and 9000 W RF power; (b) The function between the N_2O/Ar flow ratios and the intensity of atomic O emission lines at 777 nm and 844 nm .

$3p^3P \rightarrow 3s^3S$ transitions respectively [40], as shown in Fig. 3(a). It can be proved from Fig. 3(b) that when $N_2O/Ar \geq 5:2$, the intensity of atomic O emission lines at 777 nm and 844 nm gradually increase with the decrease of N_2O/Ar flow ratio. When N_2O/Ar flow ratio reaches to $5:2$, the intensity of atomic O emission lines reach the maximum value, indicating the highest concentration of atomic O has obtained at this flow ratio [29]. As the N_2O/Ar flow ratio continues decreasing, the intensity of atomic O emission line begins to decrease, which may be related to the decrease of atomic O concentration caused by the excessive dilution of N_2O by Ar.

Since N_2O dissociation in a N_2O plasma discharge occurs via electron impact [41–43]:



The Ar metastable state (Ar^*) may provide an additional way for the dissociation of N_2O and the generation of atomic O in N_2O/Ar plasma. The addition of Ar makes the dissociation of N_2O occur via Penning reactions with Ar^* [38]:



Due to the existence of this reaction, the atomic O yield by plasma-assisted N_2O/Ar oxidation will be higher than that of plasma-assisted N_2O oxidation under appropriate N_2O/Ar flow ratio. Therefore, it can be explained that the intensity of O emission line increases with the decrease of N_2O/Ar flow ratio when $N_2O/Ar \geq 5:2$ in Fig. 3(b). When the flow ratio of N_2O/Ar reaches to $5:2$, the dissociation of N_2O is basically completed and the concentration of O atom reaches the maximum value. Meanwhile, the intensity of atomic O emission line reaches the maximum. Further increase of Ar flow can not increase the atomic O yield, but it will dilute the process gases and lead to the decrease of atomic O concentration, so the intensity of atomic O emission line gradually decreased when $N_2O/Ar < 5:2$.

3.2. Influences of PANO SiO_x on doping profiles

The doping profiles, which is strongly influenced by the SiO_x

interfacial layer, is essential to achieve high performing polysilicon passivated contacts [44–46]. Fig. 4(a) shows the doping profiles (measured by ECV) based on PANO SiO_x/poly-Si(n⁺) passivated contact structures (using a fixed N_2O flow of 5 slm) with different N_2O/Ar gas flow ratios. A constant phosphorus doping level of $\sim 5 \times 10^{20}\text{ cm}^{-3}$ are observed in the poly-Si layer at $920\text{ }^\circ\text{C}$ annealing temperature for all samples, including the reference sample of plasma-assisted N_2O oxidation(PANO) SiO_x ($N_2O/Ar=5:0$). However, it is interesting to note that the doping levels within the crystalline silicon substrates are different for samples with the various SiO_x layers prepared by different N_2O/Ar flow ratios. The shallowest doping depth is found in the sample of PANO SiO_x, and with the decreasing of N_2O/Ar flow ratios, the doping depth gradually increases, the deepest doping depth is obtained when $N_2O/Ar=5:10$. This may be caused by (1) the gradually decreasing flow ratio of N_2O/Ar reduces the thickness of SiO_x layer (from 1.76 nm to 0.82 nm , as shown in Fig. 2(a)), which leads to the decrease of its ability to prevent phosphorus diffusion [47]; (2) The decrease of O concentration leads to the quality of SiO_x layer decreases, as shown in Fig. 3(b), and it also may leads to the increase of defects in SiO_x film, thus reducing the blocking ability of phosphorus diffusion in SiO_x film. In Fig. 4 (b), it can be found that the sheet resistances (R_{sh}) measured by four probes tester decreases with the increase of Ar flow. The lowest R_{sh} of $42.04\text{ }\Omega/\square$ is obtained when the $N_2O/Ar=5:10$ (the thickness of SiO_x is 0.82 nm), and the highest R_{sh} of $53.3\text{ }\Omega/\square$ is obtained from a sample of PANO SiO_x ($N_2O/Ar=5:0$, the thickness of SiO_x is 1.76 nm). The decrease of R_{sh} is mainly attributed to the internal diffusion of phosphorus, and as the phosphorus diffuse deeper into the silicon substrate, the lower R_{sh} is obtained. In addition, it also can be found from Fig. 4 (b) that the addition of Ar can significantly improve the uniformity of R_{sh} distribution, which may be the addition of Ar improves the uniformity of PANO SiO_x (as shown in Fig. 2), so that its internal diffusion can be consistent. We conclude that PANO SiO_x ($\sim 1.24\text{ nm}$) at an appropriate N_2O/Ar flow ratio ($N_2O/Ar = 5:2$) can not only form a strong phosphorus diffusion barrier, but also can form an appropriate SiO_x thickness that benefit carrier transporting. This may be caused by following reasons: 1) The addition of Ar will increase the concentration of atomic O, so the Si–O–Si bond absorption peak in SiO_x is stronger under the flow ratio of

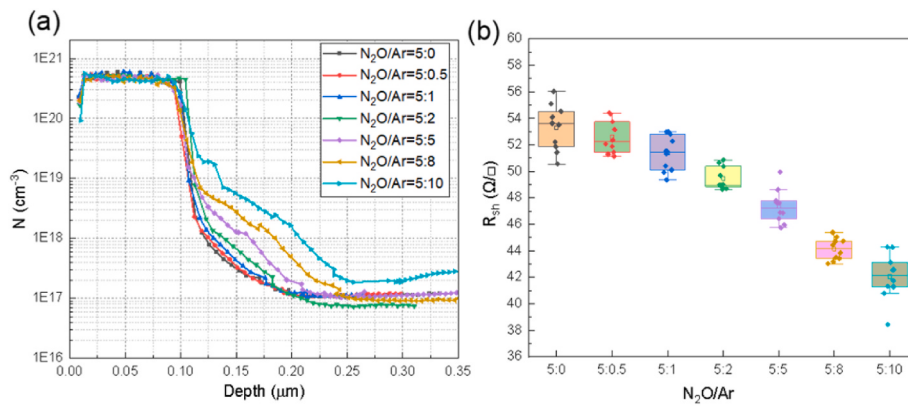


Fig. 4. (a) Doping profiles and (b) R_{sh} distribution of $\text{SiO}_x/\text{poly-Si}(n^+)$ passivated contact structure at different $\text{N}_2\text{O}/\text{Ar}$ gas flow ratios.

$\text{N}_2\text{O}/\text{Ar} = 5:2$ than that of flow ratios, and the stoichiometric configuration is close to SiO_2 [37–39], thus the high temperature resistance ability can be enhanced. 2) N or other impurities may be introduced into the SiO_x layer to improve the electrical properties and thermal stability of the poly-Si passivated contact [2,44].

The doping concentration and R_{sh} of the samples with $\text{N}_2\text{O}/\text{Ar} = 5:2$ flow ratio are further studied as a function of annealing temperatures, as shown in Fig. 5. The R_{sh} slightly decreases from $64.63 \Omega/\square$ to $49.43 \Omega/\square$ when the annealing temperature increases from 860°C to 920°C , but the R_{sh} drops sharply to $26.76 \Omega/\square$ when the annealing temperature rises to 940°C . This is mainly because the fact that when the annealing temperature $\leq 920^\circ\text{C}$, the PANAO SiO_x can effectively prevent the diffusion of phosphorus atoms into the silicon substrate. The reasons of R_{sh} declining slightly are: 1) the phosphorus doping concentration in poly-Si increase from $1.8 \times 10^{20} \text{ cm}^{-3}$ at 860°C to $5.1 \times 10^{20} \text{ cm}^{-3}$ at 920°C . The increase of phosphorus doping concentration is related to the increasing of annealing temperature which increasing the activation of phosphorus atoms. 2) Internal diffusion of phosphorus atoms lead to a decrease of R_{sh} (doping profiles at 900°C and 920°C in Fig. 5(a)). When the annealing temperature reaches to 940°C or above, the PANAO SiO_x layer no longer acts as a good diffusion barrier for phosphorus atoms. We believe that more pinholes are generated in the PANAO SiO_x layer and a large degree of film break-up has occurred at this temperature, similar to the break-up phenomenon observed in chemical silicon oxide [45], resulting in the ECV doping profiles at 940°C as shown in Fig. 5(a). Phosphorus atoms penetrate the PANAO SiO_x and diffuse into silicon substrate in large quantities, leading to the increase of recombination center in silicon substrate, finally resulting in a sharp decline of R_{sh} and poor passivation quality. This indicates that there is an optimal annealing temperature for the PANAO SiO_x layer to achieve a balance between passivation quality and carrier transport.

3.3. Effects of PANAO SiO_x on passivation quality

Fig. 6 shows the electrical properties such as minority lifetime (τ), implied open circuit voltage (iV_{oc}), single-side saturated recombination current density (J_0) and contact resistivity ($\rho_{contact}$) of poly-Si passivated contact structures with PANAO SiO_x layers prepared by 7 different $\text{N}_2\text{O}/\text{Ar}$ flow ratios as described in Section 3.2. The τ , iV_{oc} and J_0 values are studied as a function of $\text{N}_2\text{O}/\text{Ar}$ gas flow ratio with the c-Si/ $\text{SiO}_x/\text{Poly-Si}(n^+)$ structures before $\text{SiN}_x:\text{H}$ deposition, after $\text{SiN}_x:\text{H}$ deposition, after sintering and after dark annealing, as shown in Fig. 6(a) (b) (c). For the c-Si/ $\text{SiO}_x/\text{Poly-Si}(n^+)$ passivated contact structures after high temperature annealing (before $\text{SiN}_x:\text{H}$ deposition on both sides), as shown in Fig. 6 (a), The highest τ (2881 μs), iV_{oc} (724.9 mV) and lowest J_0 (7.11 fA/cm^2) are obtained in the sample of $\text{N}_2\text{O}/\text{Ar}=5:2$ flow ratio. The increase of Ar flow leads to the decrease of iV_{oc} and the increase of J_0 . When $\text{N}_2\text{O}/\text{Ar}=5:10$ flow ratio, the lowest τ and iV_{oc} and the highest J_0 are obtained. The highest τ , iV_{oc} values and the lowest J_0 values of the c-Si/ $\text{SiO}_x/\text{Poly-Si}(n^+)$ passivated contact samples after dark annealing are obtained in the $\text{N}_2\text{O}/\text{Ar}=5:2$ samples ($\tau=5751\mu\text{s}$, $iV_{oc}=741.3 \text{ mV}$, $J_0=4.79 \text{ fA/cm}^2$). The above results caused by the fact that the thickness of the PANAO SiO_x film decreases with the increase of Ar flow when $\text{N}_2\text{O}/\text{Ar}\leq 5:2$ (as shown in Fig. 2), but the addition of Ar will increase the concentration of atomic O (as shown in Fig. 3), which may lead to the formation of SiO_x closer to the stoichiometric configuration of SiO_2 . This PANAO SiO_x film contained more Si^{4+} component, and higher Si^{4+} component may lead to lower interfacial defect state, so the passivation quality is better [18]. Therefore, there are more stable chemical structure and passivation quality under the condition of $\text{N}_2\text{O}/\text{Ar}=5:2$ flow ratio, resulting in higher τ and iV_{oc} values. However, the thickness of PANAO SiO_x layer decreases to less than 1 nm with the increasing of Ar flow ratio when $\text{N}_2\text{O}/\text{Ar} > 5:2$ flow ratio, which leads to the decrease of

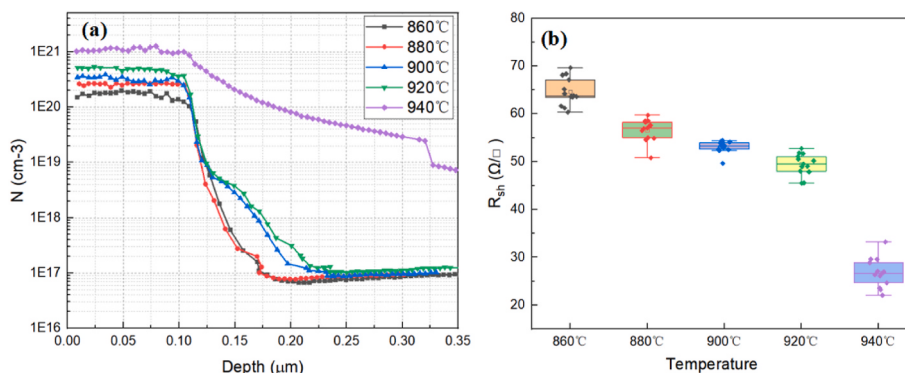


Fig. 5. (a) Doping profiles and (b) R_{sh} distribution of PANAO $\text{SiO}_x/\text{poly-Si}(n^+)$ passivated contact structures at different annealing temperatures under $\text{N}_2\text{O}/\text{Ar} = 5:2$ flow ratio.

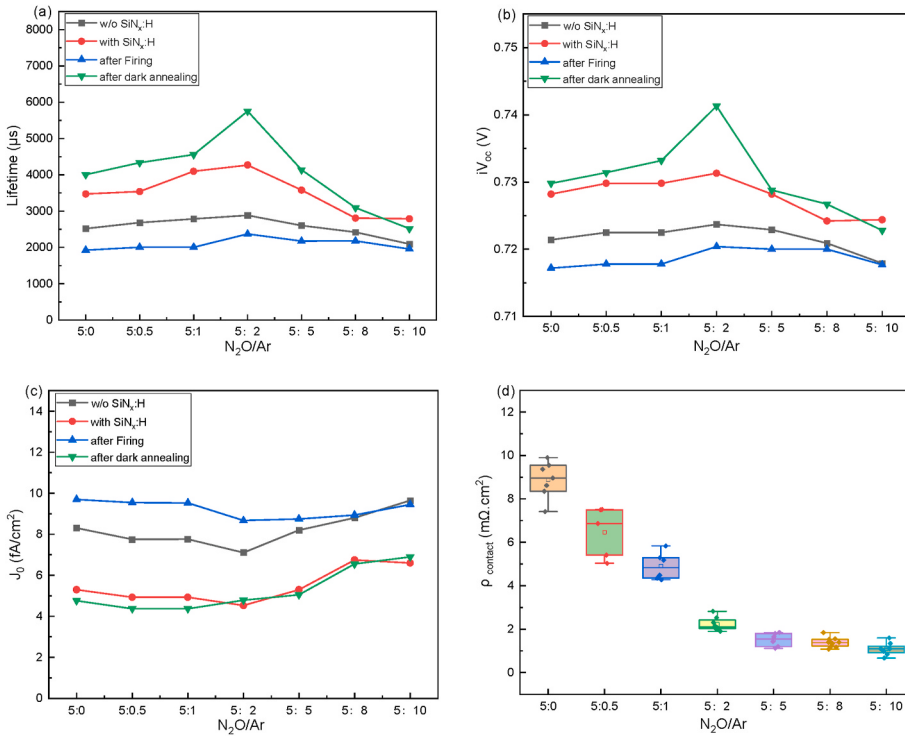


Fig. 6. The (a) τ , (b) iV_{oc} , (c) J_0 and (d) ρ_{contact} of PANAO $\text{SiO}_x/\text{poly-Si}(n^+)$ passivated contact structures prepared by different N_2O/Ar gas flow ratios at an annealing temperature of 920 °C. Tests are conducted before and after deposition of SiN_xH , after sintering and dark annealing.

its ability to prevent the phosphorus diffusion into the silicon substrate. As a result, phosphorus atoms act as the composite center in silicon substrate which decrease the passivation quality. In addition, the bombardment effect of Ar^+ on PANAO SiO_x film is also enhanced as the Ar flow increased, which leading to the increase of defects in PANAO SiO_x film, thus degenerating the passivation quality. The τ and iV_{oc} values of the samples with the shallowest doping profile of PANAO SiO_x after dark annealing are 4000 μs and 729.8 mV, respectively. The possible reasons is: in the process of PANO, there are lower atomic O concentration than PANAO process, which lead to interfacial defects in SiO_x layer and therefore resulting the decrease of chemical passivation quality. The τ and iV_{oc} values of PANAO SiO_x sample with $N_2O/Ar=5:10$ after dark annealing are 2516 μs and 722.8 mV, respectively. The possible reasons for the lower τ and iV_{oc} values are as follows: 1) the decrease of N_2O/Ar flow ratio leads to the decrease of N_2O concentration and the decrease of O atom concentration per unit volume, which makes the thickness of PANAO SiO_x thinner and thinner, and the increasing of defects in the PANAO SiO_x film lead to the decreasing of chemical passivation quality. 2) The increase of Ar flow result in the increasing of pinhole density and defects density in PANAO SiO_x film, and deteriorating film density, which may originated from the increasing of Ar^+ bombardment in the process of plasma deposition (Ar atomic emission intensity was increased as the Ar flow increased, as shown in Fig. 2), thus resulting in a decline in its ability to prevent the phosphorus diffusion, as a result, there are more impurities penetrated into the silicon substrate, which lead to the increasing of recombination center, and the decreasing of passivation quality.

We also have to ensure that the low ρ_{contact} value is capable of selective carrier transport through the PANAO SiO_x tunnel layer after we have evaluated the quality of passivation contact by τ , iV_{oc} and J_0 values. In this work, TLM is used to test the contact resistivity value to evaluate the carrier transmission characteristics (effective contact resistivity ρ_{contact}), as shown in Fig. 6(d). For PANAO $\text{SiO}_x/\text{Poly-Si}(n^+)$ passivated contact, the average contact resistivity gradually decreases with the decrease of the N_2O/Ar flow ratio. ρ_{contact} decrease from 8.88

$\text{m}\Omega\text{cm}^2$ (PANO SiO_x) to 1.09 $\text{m}\Omega\text{cm}^2$ (PANO SiO_x of $N_2O/Ar=5:10$), which may be due to the deeper penetration of phosphorus into the silicon substrate, resulting in better metal contact and higher carrier transport efficiency. However, this can also have an adverse effect on the recombination current in contact with the nonmetallic area. In addition, the thicker SiO_x layer may also lead to higher contact resistivity. Although lower contact resistivity can lead to better metal contact, it may lead to the decline of contact passivation quality in the nonmetallic area, so we should find a balance between ρ_{contact} and passivation quality [48]. At present, the average contact resistivity of PANAO $\text{SiO}_x/\text{Poly-Si}(n^+)$ passivated contact prepared under the $N_2O/Ar=5:2$ flow ratio is 2.23 $\text{m}\Omega\text{cm}^2$, it can achieve both excellent passivation quality and low contact resistivity which can meet the requirements for the preparation of high-efficiency TOPCon solar cells. The best PANAO SiO_x deposition results are obtained under the condition of $N_2O/Ar=5:2$ based on the results of τ (5750 μs), iV_{oc} (741.3 mV), J_0 (4.79 fA/cm^2) and contact resistivity ρ_{contact} (2.23 $\text{m}\Omega\text{cm}^2$).

In addition, the electrical properties of PANAO SiO_x samples with $N_2O/Ar = 5:2$ are further investigated as a function of annealing temperatures, as shown in Fig. 7. The relationship between the τ , iV_{oc} and J_0 with annealing temperature of $\text{SiO}_x/\text{poly-Si}(n^+)$ passivated contact structure before SiN_xH deposition, after SiN_xH deposition, after sintering and after dark annealing (N_2O flow was fixed at 5 slm) are tested respectively. It can be found that the values of τ and iV_{oc} increase and the values of J_0 decrease as the increase of annealing temperature when the temperature(T) ≤ 920 °C. The best passivation quality after dark annealing is achieved at 920 °C($\tau=5750$ μs , $iV_{oc}=741.3$ mV and $J_0=4.79$ fA/cm^2). We suggest that the following aspects will be considered as the reason to explained above phenomenon: 1) the chemical passivating improvement of interface SiO_x and the increase of annealing temperature enhance the absorption of impurities [18,49]; 2) The formation of positive fixed charges (Q_{tot}) at higher temperatures reduces the surface recombination of excess carriers (by repelling holes from the surface). The higher the temperature, the higher fixed charge is formed [50]; 3) An appropriate internal diffusion profile can achieve

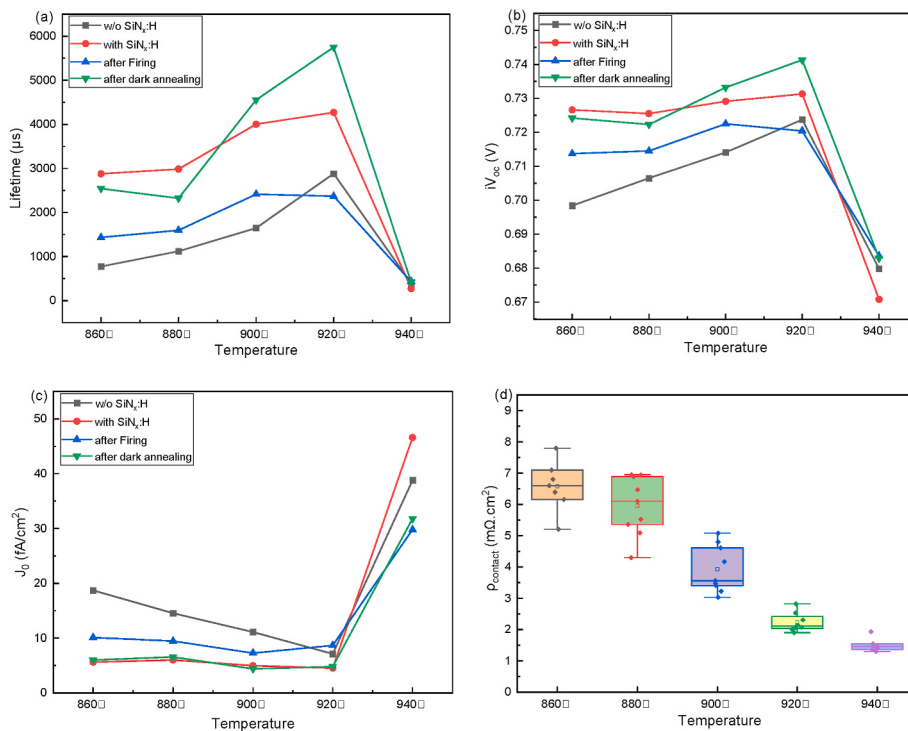


Fig. 7. The (a) τ , (b) iV_{oc} , (c) J_0 , (d) $\rho_{contact}$ of PANAO SiO_x /poly-Si(n^+) passivated contact structures at different annealing temperatures, Tests are conducted before and after deposition of $SiN_x:H$, after sintering and dark annealing.

excellent surface passivation [25]; 4) The increase of the phosphorus doping concentration in the poly-Si layer plays a major role with an increased field effect passivation that impact the lifetime, iV_{oc} and J_0 and this also explain the reduction of the contact resistivity. Si-O bond will be damaged when the annealing temperature is higher than 920 °C, resulting in anoxic defects. The SiO_x layer may also damaged during high-temperature annealing, resulting in a sharp decline in passivation quality. We attribute this behavior to the fact that the pinhole density of the SiO_x layer increases sharply or SiO_x film breaks at a higher annealing temperature, which leads to severe internal diffusion of phosphorus. As shown in Fig. 5(a), phosphorus atoms penetrate SiO_x and diffuse into the silicon substrate in large numbers, resulting in the increase of potential recombination centers in the silicon substrate and the decrease of chemical passivating effect. The above reasons deteriorate the passivation quality sharply. In addition, it can be seen from Fig. 6(d) that the contact resistivity decreases with the increase of annealing temperature, which is mainly related to the internal diffusion of phosphorus [18,25].

3.4. Effects of PANAO SiO_x on electrical performance of TOPCon solar cells

We have prepared PANAO SiO_x and its corresponding TOPCon solar cells under different N_2O/Ar flow ratios as above, the electrical performance are shown in Table 1. It can be found that the average conversion

efficiency increases first and then decreases with the increase of Ar flow. The average conversion efficiency reaches to the highest 24.81% under the condition of $N_2O/Ar= 5:2$, which is mainly attributed to the increase of open circuit voltage (V_{oc}) and filling factor (FF), which reach to 0.7092 V and 84.45, respectively. The increase of V_{oc} and FF is mainly related to the improvement of passivation quality and the decrease of contact resistivity, as described in Section 3.3. In addition, under the condition of $N_2O/Ar=5:2$, we also obtain the champion efficiency of 25.06%. The specific electrical parameters are $V_{oc}=0.7132$ V, $I_{sc}=13.7239$ A, FF=84.55, as shown in Fig. 8.

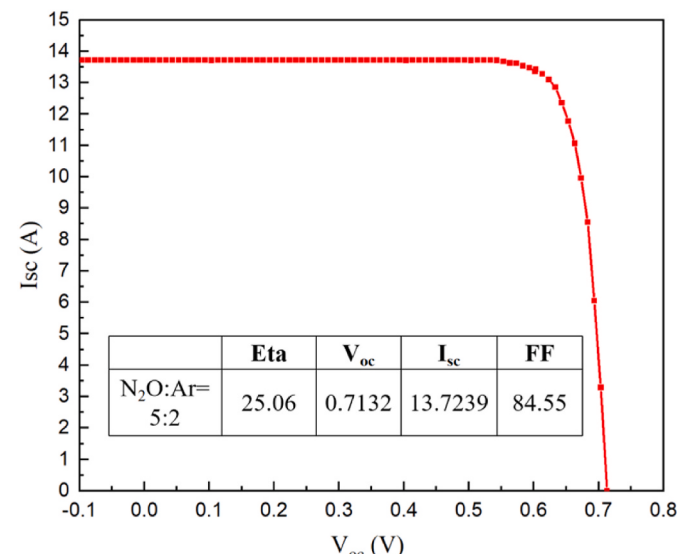


Fig. 8. I-V curve of champion solar cell at $N_2O/Ar= 5:2$.

Table 1
Electrical parameters of TOPCon solar cells prepared under different N_2O/Ar flow ratios.

	Counts	Eta (%)	V_{oc} (V)	I_{sc} (A)	FF
$N_2O:Ar=5:0$	556	24.43	0.7058	13.7125	83.61
$N_2O:Ar=5:0.5$	567	24.48	0.7065	13.7069	83.73
$N_2O:Ar=5:1$	521	24.58	0.7083	13.6857	83.99
$N_2O:Ar=5:2$	587	24.81	0.7092	13.7231	84.45
$N_2O:Ar=5:5$	566	24.72	0.7086	13.6998	84.36
$N_2O:Ar=5:8$	579	24.61	0.7078	13.7018	84.05
$N_2O:Ar=5:10$	576	24.45	0.7048	13.6592	84.13

4. Conclusion

In summary, in order to improve the uniformity of SiO_x prepared by plasma-assisted N₂O oxidation method and the passivation quality of SiO_x/poly-Si(n⁺) passivation contact structure, we had adopted the plasma-assisted N₂O/Ar oxidation method to improve the concentration of O atoms in the deposition process, and prepared PANAO SiO_x with excellent quality, achieving excellent electrical performance.

We found that decreasing the N₂O/Ar flow ratios from 5:0 to 5:2 can significantly improve the atomic O concentration during the PANAO SiO_x film deposition process. Thus the stoichiometric configuration of prepared SiO_x film was closed to SiO₂, and the high temperature resistance was enhanced. For a precise control of the thickness of such thin SiO_x interfacial layers, a higher Ar flow was beneficial as it lowers the deposition rate. We found that a chemically stable, uniform and optimum thickness of SiO_x could be achieved by using gas flow ratio of N₂O/Ar=5:2. The highest τ and iV_{oc} with 5751 μ s and 741.3 mV and lowest J_0 and low $\rho_{contact}$ with 4.79 fA/cm² and 2.23 m Ω /cm² and champion efficiency of 25.06% were obtained at the flow ratio of N₂O/Ar= 5:2. It was expected that by further optimising the doping process, the annealing condition and the hydrogenation step, excellent PANAO SiO_x based poly-Si passivated contacts and efficiency of TOPCon solar cells could be achieved.

CRediT authorship contribution statement

Jiabin Huang: Writing – review & editing, Writing – original draft, Investigation. **Zengchao Zhao:** Writing – review & editing, Formal analysis, Conceptualization. **Ming Li:** Project administration, Investigation, Data curation. **Jun Chen:** Validation, Investigation. **Xiaorong Zhou:** Methodology, Formal analysis. **Xinxin Deng:** Software, Investigation, Data curation. **Bin Li:** Data curation, Formal analysis. **Kailin Shen:** Resources, Investigation. **Qiuyun Cheng:** Investigation, Formal analysis, Conceptualization. **Xianwu Cai:** Supervision, Resources, Formal analysis, Conceptualization.

Declaration of competing interest

The authors declare that they have no known competing financial interests or personal relationships that could have appeared to influence the work reported in this paper.

Data availability

Data will be made available on request.

Acknowledgements

This work was supported by the Hunan innovative province construction project - Crystalline silicon solar cell engineering technology center (2019TP2048) . Facilities at the Hunan Red Solar Photo-electricity Science and Technology Co., Ltd. were used for the film deposition and thickness measurements. The authors would like to thank the Sany Silicon Energy (Zhuzhou) Co., Ltd. for providing the test of TOPCon solar cells.

References

- [1] W. Stefan, B. Glunz, J. Steinhauser, I. Polzin, C. Luderer, F. Feldmann, Silicon-based passivating contacts: the TOPCon Route, *Prog. Photovolt. Res. Appl.* (2021) 1–19, <https://doi.org/10.1002/pip.3522>.
- [2] M. Stöhr, J. Aprojanz, R. Brendel, T. Dullweber, Firing-stable PECVD SiO_xN_y/n-poly-Si surface passivation for silicon solar cells, *ACS Appl. Energy Mater.* 4 (5) (2021) 4646–4653, <https://doi.org/10.1021/acsaeam.1c00265>.
- [3] F. Feldmann, M. Bivour, C. Reichel, M. Hermle, S.W. Glunz, A passivated rear contact for high-efficiency N-type Si solar cells enabling high V_{oc} s and FF > 82, in: *Proceedings 28th European Photovoltaic Solar Energy Conference*, 2013, pp. 988–992.
- [4] A. Richter, R. Müller, J. Benick, F. Feldmann, S.W. Glunz, Design rules for high-efficiency both-sides-contacted silicon solar cells with balanced charge carrier transport and recombination losses, *Nat. Energy* 6 (2021) 429–438, <https://doi.org/10.1038/s41560-021-00805-w>.
- [5] F. Haase, C. Hollemann, S. Schäfer, A. Merkle, M. Rienäcker, J. Krügener, R. Brendel, R. Peibst, Laser contact openings for local poly-Si-metal contacts enabling 26.1%-efficient POLO-IBC solar cells, *Sol. Energy Mater. Sol. Cell.* 186 (2018) 184–193, <https://doi.org/10.1016/j.solmat.2018.06.020>.
- [6] F. Feldmann, M. Bivour, C. Reichel, M. Hermle, S.W. Glunz, Passivated rear contacts for high-efficiency n-type Si solar cells providing high interface passivation quality and excellent transport characteristics, *Sol. Energy Mater. Sol. Cells* 120 (2014) 270–274, <https://doi.org/10.1016/j.solmat.2013.09.017>.
- [7] A. Richter, J. Benick, F. Feldmann, A. Fell, M. Hermle, S.W. Glunz, N-type Si solar cells with passivating electron contact: identifying sources for efficiency limitations by wafer thickness and resistivity variation, *Sol. Energy Mater. Sol. Cells* 173 (2017) 96–105, <https://doi.org/10.1016/j.solmat.2017.05.042>.
- [8] C. Reichel, F. Feldmann, R. Mueller, R.C. Reedy, B.G. Lee, D.L. Young, P. Stradins, M. Hermle, S.W. Glunz, Tunnel oxide passivated contacts formed by ion implantation for applications in silicon solar cells, *J. Appl. Phys.* 118 (2015) 491, <https://doi.org/10.1063/1.4936223>.
- [9] F. Feldmann, M. Simon, M. Bivour, C. Reichel, M. Hermle, S.W. Glunz, Efficient carrier-selective p- and n-contacts for Si solar cells, *Sol. Energy Mater. Sol. Cells* 131 (2014) 100–104, <https://doi.org/10.1016/j.solmat.2014.05.039>.
- [10] Z. Zhang, Y. Zeng, C.-S. Jiang, Y. Huang, M. Liao, H. Tong, M. Al-Jassim, P. Gao, C. Shou, X. Zhou, B. Yan, J. Ye, Carrier transport through the ultrathin silicon-oxide layer in tunnel oxide passivated contact (TOPCon) c-Si solar cells, *Sol. Energy Mater. Sol. Cells* 187 (2018) 113–122, <https://doi.org/10.1016/j.solmat.2018.07.025>.
- [11] F. Feldmann, M. Bivour, C. Reichel, H. Steinkemper, M. Hermle, S.W. Glunz, Tunnel oxide passivated contacts as an alternative to partial rear contacts, *Sol. Energy Mater. Sol. Cells* 131 (2014) 46–50, <https://doi.org/10.1016/j.solmat.2014.06.015>.
- [12] S. Duttagupta, N. Nandakumar, P. Padhamnath, J.K. Batis, R. Stangl, A.G. Aberle, monoPoly™ cells: large-area crystalline silicon solar cells with fire-through screen printed contact to doped polysilicon surfaces, *Sol. Energy Mater. Sol. Cells* 187 (2018) 76–81, <https://doi.org/10.1016/j.solmat.2018.05.059>.
- [13] Y. Tao, K. Madani, E. Cho, B. Rounsvaille, V. Upadhyaya, A. Rohatgi, High-efficiency selective boron emitter formed by wet chemical etch-back for n-type screen-printed Si solar cells, *Appl. Phys. Lett.* 110 (2017), 021101, <https://doi.org/10.1063/1.4973626>.
- [14] H. Kobayashi Asuka, O. Maida, M. Takahashi, H. Iwasa, Nitric acid oxidation of Si to form ultrathin silicon dioxide layers with a low leakage current density, *J. Appl. Phys.* 94 (2003) 7328–7335, <https://doi.org/10.1063/1.1621720>.
- [15] H. Tong, M. Liao, Z. Zhang, Y. Wan, D. Wang, C. Quan, L. Cai, P. Gao, W. Guo, H. Lin, C. Shou, Y. Zeng, B. Yan, J. Ye, A strong-oxidizing mixed acid derived high-quality silicon oxide tunneling layer for polysilicon passivated contact silicon solar cell, *Sol. Energy Mater. Sol. Cells* 188 (2018) 149–155, <https://doi.org/10.1016/j.solmat.2018.09.001>.
- [16] R. van der Vossen, F. Feldmann, A. Moldovan, M. Hermle, Comparative study of differently grown tunnel oxides for p-type passivating contacts, *Energy Proc.* 124 (2017) 448–454, <https://doi.org/10.1016/j.egypro.2017.09.273>.
- [17] D. Yan, A. Cuevas, J. Bullock, Y. Wan, C. Samundsett, Phosphorus-diffused polysilicon contacts for solar cells, *Sol. Energy Mater. Sol. Cell.* 142 (2015) 75–82, <https://doi.org/10.1016/j.solmat.2015.06.001>.
- [18] X. Guo, M. Liao, Z. Rui, Q. Yang, Z. Wang, C. Shou, W. Ding, X. Luo, Y. Cao, J. Xu, L. Fu, Y. Zeng, B. Yan, J. Ye, Comparison of different types of interfacial oxides on hole-selective p⁺-poly-Si passivated contacts for high-efficiency c-Si solar cells, *Sol. Energy Mater. Sol. Cells* 210 (2020), 110487, <https://doi.org/10.1016/j.solmat.2020.110487>.
- [19] A. Moldovan, F. Feldmann, K. Kaufmann, S. Richter, M. Hermle, Tunnel oxide passivated carrier-selective contacts based on ultra-thin SiO₂ layers grown by photo-oxidation or wet-chemical oxidation in ozonized water, in: *IEEE 42nd Photovoltaic Specialist Conference (PVSC)*, 2015, 15664433, <https://doi.org/10.1109/PVSC.2015.7356144>.
- [20] Z. Liu, N. Lin, Q. Zhang, B. Yang, L. Xie, Y. Chen, W. Li, M. Liao, H. Chen, W. Liu, Y. Wang, S. Huang, B. Yan, Y. Zeng, Y. Wan, J. Ye, 24.4% industrial tunnel oxide passivated contact solar cells with ozone-gas oxidation Nano SiO_x and tube PECVD prepared in-situ doped polysilicon, *Sol. Energy Mater. Sol. Cells* 243 (2022), 111803, <https://doi.org/10.1016/j.solmat.2022.111803>.
- [21] M. Lozac'h, S. Nunomura, K. Matsubara, Double-sided TOPCon solar cells on textured wafer with ALD SiO_x layer, *Sol. Energy Mater. Sol. Cells* 207 (2020), 110357, <https://doi.org/10.1016/j.solmat.2019.110357>.
- [22] D. Hiller, P. Hnicke, D. Knig, Material combination of Tunnel-SiO₂ with a (sub-) Monolayer of ALD-AlO_x on silicon offering a highly passivating hole selective contact, *Sol. Energy Mater. Sol. Cells* 215 (2020), 110654, <https://doi.org/10.1016/j.solmat.2020.110654>.
- [23] S.P. Padi, M.Q. Khokhar, S. Chowdhury, Nanoscale SiO_x tunnel oxide deposition techniques and their influence on cell parameters of TOPCon solar cells, *Transactions on Electrical and Electronic Materials* 22 (2021) 557–566.
- [24] H. Yousuf, M.Q. Khokhar, M.A. Zahid, Tunnel oxide deposition techniques and their parametric influence on nano-scaled SiO_x layer of TOPCon solar cell: a review, *Energies* 15 (2022) 5753.
- [25] Y. Huang, M. Liao, Z. Wang, X. Guo, C. Jiang, Q. Yang, Z. Yuan, D. Huang, J. Yang, X. Zhang, Q. Wang, H. Jin, M. Al-Jassim, C. Shou, Y. Zeng, B. Yan, J. Ye, Ultrathin silicon oxide prepared by in-line plasma-assisted N₂O oxidation (PANO) and the

- application for n-type polysilicon passivated contact, Sol. Energy Mater. Sol. Cells 208 (2020), 110389, <https://doi.org/10.1016/j.solmat.2019.110389>.
- [26] A. Masuda, Y. Yonezawa, A. Morimoto, M. Kumeda, T. Shimizu, Ultrathin SiO₂ films on Si formed by N₂O-plasma oxidation technique, Appl. Surf. Sci. 81 (1994) 277–280, [https://doi.org/10.1016/0169-4332\(94\)90284-4](https://doi.org/10.1016/0169-4332(94)90284-4).
- [27] H. Kim, S. Bae, K.S. Ji, S.M. Kim, J.W. Yang, C.H. Lee, K.D. Lee, S. Kim, Y. Kang, H. S. Lee, Passivation properties of tunnel oxide layer in passivated contact silicon solar cells, Appl. Surf. Sci. 409 (2017) 140–148, <https://doi.org/10.1016/j.apsusc.2017.02.195>.
- [28] T. Gao, Q. Yang, X. Guo, Y. Huang, Z. Zhang, Z. Wang, M. Liao, C. Shou, Y. Zeng, B. Yan, G. Hou, X. Zhang, Y. Zhao, J. Ye, An industrially viable TOPCon structure with both ultra-thin SiOx and n+ -poly-Si processed by PECVD for p-type c-Si solar cells, Sol. Energy Mater. Sol. Cells 200 (2019), 109926, <https://doi.org/10.1016/j.solmat.2019.109926>.
- [29] B.C. Smith, A. Khandelwal, H.H. Lamb, Ar/N₂O remote plasma-assisted oxidation of Si(100): plasma chemistry, growth kinetics, and interfacial reactions, J. Vac. Sci. Technol. B 18 (3) (2000) 1757, <https://doi.org/10.1116/1.591467>.
- [30] G. Lucovsky, D.V. Tsu, R.J. Markunas, in: S.M. Roesnagel, J.J. Cuomo, W. D. Westwood (Eds.), Handbook of Plasma Processing Technology, vol. 87, Noyes, Park Ridge, NJ, 1990.
- [31] S.R. Kaluri, D.W. Hess, Constant current N₂O plasma anodization of silicon, J. Electrochem. Soc. 144 (1997) 2200, <https://doi.org/10.1149/1.1837765>.
- [32] L.M. Landsberger, R. Ghayour, M. Sayedi, M. Kahrizi, D. Landheer, J.A. Bardwell, Y. Riopel, C. Jean, V. Loguidice, Electrical characterization of metal-oxide-semiconductor capacitors with anodic and plasma-nitrided oxides, J. Vac. Sci. Technol. A 18 (2000) 676, <https://doi.org/10.1116/1.582250>.
- [33] Y. Saito, Oxynitridation of silicon by remote-plasma excited nitrogen and oxygen, Appl. Phys. Lett. 68 (1996) 800, <https://doi.org/10.1063/1.116537>.
- [34] D.R. Lee, G. Lucovsky, M.S. Denker, C. Magee, Nitrogen-atom incorporation at Si-SiO₂ interfaces by a low-temperature(300°C), pre-deposition, remote-plasma oxidation using N₂O, J. Vac. Sci. Technol. 13 (1995) 1671, <https://doi.org/10.1116/1.579749>.
- [35] A.J. Batey, E. Tierney, J. Stasiak, T.N. Nguyen, Plasma-enhanced CVD of high quality insulating films, Appl. Surf. Sci. 39 (1) (1989) 1–15, [https://doi.org/10.1016/0169-4332\(89\)90415-7](https://doi.org/10.1016/0169-4332(89)90415-7).
- [36] G. Lucovsky, D.V. Tsu, S.S. Kim, R.J. Markunas, G.G. Fountain, Formation of thin film dielectrics by remote plasma-enhanced chemical-vapor deposition (remote PECVD), Appl. Surf. Sci. 39 (1989) 33, [https://doi.org/10.1016/0169-4332\(89\)90418-2](https://doi.org/10.1016/0169-4332(89)90418-2).
- [37] D.L. Smith, A.S. Alimonda, Chemistry of SiO₂ plasma deposition, J. Electrochem. Soc. 140 (1993) 1496, <https://doi.org/10.1149/1.2221586>.
- [38] C.H. Courtney, B.C. Smith, H.H. Lamb, Remote plasma-enhanced chemical vapor deposition of SiO₂ using Ar/N₂O and SiH₄, J. Electrochem. Soc. 145 (1998) 3957, <https://doi.org/10.1149/1.1838898>.
- [39] J.A. Goleb, in: J.A. Dean, T.C. Rains (Eds.), Flame Emission and Atomic Absorption Spectrometry, Marcel Dekker, New York, 1975.
- [40] R.E. Walkup, K.L. Saenger, G.S. Selwyn, Studies of atomic oxygen in O₂+CF₄ rf discharges by twophoton laser induced fluorescence and optical emission spectroscopy, J. Chem. Phys. 84 (1986) 2668, <https://doi.org/10.1063/1.450339>.
- [41] L.G. Piper, W.T. Rawlins, O-atoms yields from microwave discharges in N₂O/Ar mixtures, J. Phys. Chem. 90 (1986) 320–325, <https://doi.org/10.1021/J100274A024>.
- [42] T.A. Cleland, D.W. Hess, Diagnostics and modeling of N₂O RF glow discharges, J. Electrochem. Soc. 136 (1989) 3103, <https://doi.org/10.1149/1.2096409>.
- [43] V. Lisovskiy, J.-P. Booth, K. Landry, D. Douai, V. Cassagne, V. Yegorenkov, Modes and the alpha-gamma transition in rf capacitive discharges in N₂O at different rf frequencies, Phys. Plasma. 13 (2006), 103505, <https://doi.org/10.1063/1.2364135>.
- [44] F. Feldmann, J. Schoen, J. Niess, W. Lerch, M. Hermle, Studying dopant diffusion from poly-Si passivating contacts, Sol. Energy Mater. Sol. Cell. 200 (2019), 109978, <https://doi.org/10.1016/j.solmat.2019.109978>.
- [45] V. Tomar, D. Patil, D. Gautam, Deposition and characterization of SiON films using HMDS for photonics applications, Semicond. Sci. Technol. 22 (2006) 43, <https://doi.org/10.1088/0268-1242/22/2/008>.
- [46] D. Yan, A. Cuevas, Y. Wan, J. Bullock, Silicon nitride/silicon oxide interlayers for solar cell passivating contacts based on PECVD amorphous silicon, Phys. Status Solidi Rapid Res. Lett. 9 (2015) 617–621, <https://doi.org/10.1002/pssr.201510325>.
- [47] Q. Wang, W. Wu, N. Yuan, Influence of SiO_x film thickness on electrical performance and efficiency of TOPCon solar cells, Sol. Energy Mater. Sol. Cell. 208 (2020), 110423, <https://doi.org/10.1016/j.solmat.2020.110423>.
- [48] Q. Wang, W. Wu, D. Chen, L. Yuan, S. Yang, Y. Sun, S. yang, Q. Zhang, Y. Cao, H. Qu N. Yuan, J. Ding, Study on the cleaning process of n⁺-poly-Si wraparound removal of TOPCon solar cells, Sol. Energy 211 (2020) 324–335, <https://doi.org/10.1016/j.solener.2020.09.028>.
- [49] Z. Wang, Z. Liu, M. Liao, D. Huang, X. Guo, Z. Rui, Q. Yang, W. Guo, J. Sheng, C. Shou, B. Yan, Z. Yuan, Y. Zeng, J. Ye, Effective gettering of in-situ phosphorus-doped polysilicon passivating contact prepared using plasma-enhanced chemical-vapor deposition technique, Sol. Energy Mater. Sol. Cells 206 (2020), 110256, <https://doi.org/10.1016/j.solmat.2019.110256>.
- [50] G. Kaur, Z. Xin, T. Dutta, R. Sridharan, R. Stangl, A. Danner, Improved silicon oxide/polysilicon passivated contacts for high efficiency solar cells via optimized tunnel layer annealing, Sol. Energy Mater. Sol. Cells 217 (2020), 110720, <https://doi.org/10.1016/j.solmat.2020.110720>.